

# An Efficient Hierarchical Zonal Method for Large-Scale Circuit Simulation and Its Real-Time Application on More Electric Aircraft Microgrid

Zhen Huang , *Student Member, IEEE*, and Venkata Dinavahi , *Senior Member, IEEE*

**Abstract**—Large-scale circuit simulation poses a challenge to most simulation tools because of its high computational complexity. This paper presents an efficient method, which decouples the circuit topology and components' characteristics in computation so as to make it suitable for large-scale circuit simulation. The proposed method is based on a circuit lemma, which indicates the relationship of branch voltages and currents. The proving process of this lemma is provided in this paper. The working principle of the proposed method is elaborated and its numerical stability is also analyzed. This method achieves nearly linear computational complexity and is very suitable for hierarchical and zonal computation. The proposed method is verified by real-time application on the more electric aircraft microgrid. Hardware-in-the-loop testing of this study case on Xilinx Virtex Ultrascale+ field programmable gate array (FPGA) board is achieved and the results are compared with PSCAD/EMTDC. The resulting waveforms from these two simulation tools show very good agreement on both normal and fault operation test scenarios, which demonstrates that the proposed method has very good performance on computational accuracy and efficiency.

**Index Terms**—Aircraft power systems, circuit modeling, circuit simulation, field programmable gate arrays, large-scale circuits, microgrid, real-time systems.

## I. INTRODUCTION

CIRCUIT simulation is essential in most of the electric system's design and validation process as it can serve as a powerful tool to reflect the electric system's behavior and properties [1], [2]. Up to now, there are basically two categories of mature algorithms in modern circuit simulation area: the nodal analysis method [3]–[6] (also known as resistive companion method, Dommel algorithm, etc.) and state-space method [7]–[12] (also known as state-variable method). The simulation program typically selects one algorithm and develops the system

Manuscript received April 10, 2018; revised August 21, 2018; accepted September 4, 2018. Date of publication September 26, 2018; date of current version February 28, 2019. This work was supported by the Natural Science and Engineering Research Council of Canada. The work of Z. Huang was supported by the China Scholarship Council. (Corresponding author: Zhen Huang.)

The authors are with the Department of Electrical and Computer Engineering, University of Alberta, Edmonton, AB T6G 2R3, Canada (e-mail: zh2@ualberta.ca; dinavahi@ualberta.ca).

Color versions of one or more of the figures in this paper are available online at <http://ieeexplore.ieee.org>.

Digital Object Identifier 10.1109/TIE.2018.2870366

matrix according to the method's corresponding modeling rule. These two methods have been validated by various circuits and both evolved mature software. Representative of nodal analysis method is PSCAD/EMTDC [13] and the state-space method is MATLAB/Simulink [14].

However, both these algorithms become computational inefficient when the circuit's scale becomes large. The reason is evident: the size of system matrix increases along with the circuit's scale. This problem is, especially severe for the nodal analysis method because it requires matrix division in every time-step. The computational complexity of direct matrix inversion is  $O(N^3)$ ; even when an advanced solver such as Gaussian elimination method is used, the complexity can only be reduced to  $O(N^3/3)$ , still in order 3 of the matrix size. As for the state-space method, the complexity depends on the discretization method. If the forward Euler method is adopted, it requires only one matrix multiplication in every time-step and the computational complexity is  $O(N^2)$ . But forward Euler method behaves poorly with respect of numerical stability. In most cases, some advanced algorithms, like Heun, or the Runge–Kutta method, have to be adopted. However, as long as the discretization method is in explicit form, the complexity will still be in order 2 of the matrix size, and once an implicit method, such as Backward Euler or Trapezoidal Rule, is chosen, the complexity will increase to order 3.

There have been various attempts to reduce the computational complexity of the circuit solution. The most natural guideline is circuit decoupling. Two successful methods have been created in the literature and implemented in many applications: latency insertion method (LIM) [15]–[17] and transmission line modeling (TLM) method [18], [19]. The basic idea of these methods is similar. They take advantage of the inductive and capacitive elements in the network to create latency between two subsystems so as to decouple them. The difference is that LIM requires inductive element along every branch and capacitive element between every node with ground, while TLM only introduces latency in several parts of the network. Thus, LIM realizes fully decoupling of the circuit network and the computational complexity reduces to linear, at the expense of modifying the circuit model because there are seldom cases when the circuit meets the requirement of LIM originally. TLM is usually used to decouple the system when solving nonlinearities or the two subsystems already have some decoupling nature such as parallel

connection by a large capacitance. Therefore, TLM can be deemed as partial decoupling of the network and traditional methods are utilized within the decoupled subsystem.

Although these two decoupling methods are successful in many applications, they still have limitations. One common deficiency is the difficulty of selecting an appropriate value of latency, especially when this latency is inserted virtually, i.e., it does not exist in the real system. If the latency is too small (which means smaller time-step), it may lose the advantage of computational efficiency. On the other hand, if the latency is too large, it may suffer from numerical instability or may distort the original circuit's transients. There is no standard way or formula for choosing the latency in literature and it is often done manually, i.e., by trial and error iteration.

Considering the aforementioned insufficiency, simulation of large-scale circuits still poses a challenge. Typically speaking, the behavior of a circuit is determined by two factors—the circuit topology and the component's characteristics. However, the traditional modeling methods often mix these two factors into one system matrix, i.e., whenever there is a change in the circuit topology or the component's characteristics, the system matrix has to be reformed. This paper presents a method that decouples these two factors and deals with them separately. This method is the extension of Zhen's work in [20], thus, it will be referred to as Enhanced Zhen's Method (EZM) henceforth. Under EZM, matrix inversion is only required when analyzing the topology. It is very easy to compute and suitable for computer programming. In most cases, the circuit topology remains unaltered in the simulation and the component's characteristics are the main stimulus of the transients. In addition, each circuit component can be handled separately as well, which reduces the computational complexity to nearly linear and very suitable for parallel computation. These features make EZM very suitable for large-scale circuit simulation.

## II. EZM MODELING METHODOLOGY

The EZM modeling methodology is based on a circuit lemma that indicates the relationship of branch voltages and currents in the circuit.

**Lemma 1:** Given a circuit that has  $n$  nodes and  $b$  branches, there exist  $n - 1$  individual branch voltages so that the other  $b - n + 1$  branch voltages can be expressed as simply addition or subtraction of these  $n - 1$  voltages and these  $n - 1$  branch currents can be expressed as simply addition or subtraction of the  $b - n + 1$  branch currents. In addition, when written in matrix form, this matrix is an antisymmetric matrix.

An example is given first to exemplify this lemma and then prove it. The topology of Fig. 1 is taken from a commonly used power electronic circuit named neutral point clamped (NPC) topology and this is a half-bridge configuration. There are six nodes denoted from  $n_0$  to  $n_5$  and nine branches denoted as  $b_1$  to  $b_9$ .

Fig. 1(a) shows one possible working mode of this circuit where switches  $b_2$  and  $b_3$  are in ON-stage, while switches  $b_1$  and  $b_4$  are in OFF-stage. Meanwhile, the current of inductor  $b_9$  flows from  $n_3$  to  $n_0$ , which makes diode  $b_5$  in ON-stage and  $b_6$  in OFF-stage.

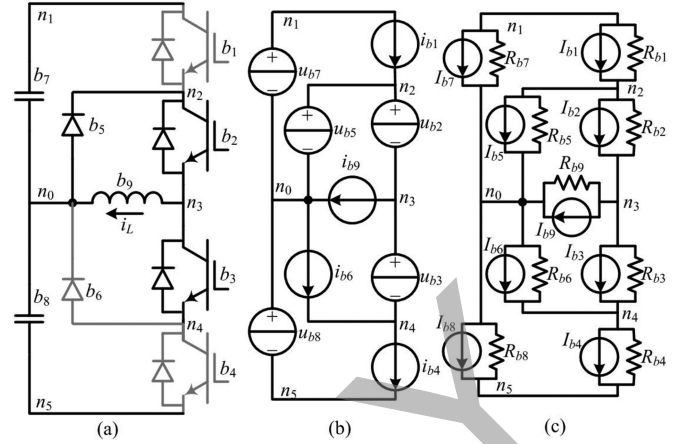


Fig. 1. NPC half-bridge topology. (a) Working mode. (b) Voltage/current source equivalent configuration. (c) Resistor companion current source equivalent configuration.

As is well-known that the circuit topology can be expressed as node–branch incidence matrix or loop–branch incidence matrix. However, the nodes in the circuit are unique, while loops are not (in other words, there is only one node–branch incidence matrix, while there are multiple loop–branch incidence matrices). This is why most simulation programs favor nodal analysis and take node voltages as computation variables, rather than Thévenin analysis and solving loop currents. The core value of Lemma 1 is providing a way to find the relationship of branch currents by simple manipulation of node–branch incidence matrix, so that the program can get rid of some complex graph concepts like trees. The following process shows how to obtain the current relationship in Fig. 1 by use of Lemma 1.

*Step 1:* Write the node–branch incidence matrix  $\mathbf{A}$

$$\mathbf{A} = \begin{bmatrix} 0 & 0 & 0 & 0 & -1 & 1 & -1 & 1 & -1 \\ 1 & 0 & 0 & 0 & 0 & 0 & 1 & 0 & 0 \\ -1 & 1 & 0 & 0 & 1 & 0 & 0 & 0 & 0 \\ 0 & -1 & 1 & 0 & 0 & 0 & 0 & 0 & 1 \\ 0 & 0 & -1 & 1 & 0 & -1 & 0 & 0 & 0 \\ 0 & 0 & 0 & -1 & 0 & 0 & 0 & -1 & 0 \end{bmatrix}. \quad (1)$$

The node–branch incidence matrix is formed in such a way that the rows and columns of  $\mathbf{A}$  correspond to the nodes and branches in the topology, respectively. The entry of  $\mathbf{A}(a_{ij})$  is 1 when node  $i$  connects to branch  $j$ 's positive end; and is  $-1$  when they interconnect at branch  $j$ 's negative end. When they have no connection in the topology, then  $\mathbf{A}(a_{ij})$  is 0.

*Step 2:* Classify the  $b$  branches and select  $n - 1$  branches as voltage sources and others as current sources. In Fig. 1,  $b_2$ ,  $b_3$ ,  $b_5$ ,  $b_7$ , and  $b_8$  are suitable to be taken as voltage sources, while  $b_1$ ,  $b_4$ ,  $b_6$ , and  $b_9$  are suitable to be taken as current sources, as shown in Fig. 1(b). Then, split matrix  $\mathbf{A}$  into two sections which correspond to the  $n - 1$  voltage sources ( $\mathbf{A}_1$ ) and  $b - n + 1$  current sources ( $\mathbf{A}_2$ ), respectively. Before doing this, delete one row of matrix  $\mathbf{A}$  since the rows of  $\mathbf{A}$  are not independent. The choice of deleted row is arbitrary. However, it is better to

choose a node which has voltage source connected to it. In this example, row 1 which corresponds to node  $n_0$  is deleted.

*Step 3:* Do matrix manipulation so as to find the voltage relationships in Lemma 1, where  $\mathbf{A}'_1$  is the transpose of  $\mathbf{A}_1$ , and is the same for other matrices.

$$\mathbf{A}_1 = \begin{bmatrix} 0 & 0 & 0 & 1 & 0 \\ 1 & 0 & 1 & 0 & 0 \\ -1 & 1 & 0 & 0 & 0 \\ 0 & -1 & 0 & 0 & 0 \\ 0 & 0 & 0 & 0 & -1 \end{bmatrix}, \mathbf{A}_2 = \begin{bmatrix} 1 & 0 & 0 & 0 \\ -1 & 0 & 0 & 0 \\ 0 & 0 & 0 & 1 \\ 0 & 1 & -1 & 0 \\ 0 & -1 & 0 & 0 \end{bmatrix}. \quad (2)$$

$$\begin{bmatrix} u_{b1} \\ u_{b4} \\ u_{b6} \\ u_{b9} \end{bmatrix} = \mathbf{A}'_2 (\mathbf{A}'_1)^{-1} \begin{bmatrix} u_{b2} \\ u_{b3} \\ u_{b5} \\ u_{b7} \\ u_{b8} \end{bmatrix} \\ = \begin{bmatrix} 0 & 0 & -1 & 1 & 0 \\ -1 & -1 & 1 & 0 & 1 \\ 1 & 1 & -1 & 0 & 0 \\ -1 & 0 & 1 & 0 & 0 \end{bmatrix} \begin{bmatrix} u_{b2} \\ u_{b3} \\ u_{b5} \\ u_{b7} \\ u_{b8} \end{bmatrix}. \quad (3)$$

*Step 4:* Rewrite (3) into full  $b \times b$  matrix form and using the antisymmetry property in Lemma 1 to supplement the section that indicates currents' relationship.

$$\begin{bmatrix} u_{b1} \\ i_{b2} \\ i_{b3} \\ u_{b4} \\ i_{b5} \\ u_{b6} \\ i_{b7} \\ i_{b8} \\ u_{b9} \end{bmatrix} = \begin{bmatrix} 0 & 0 & 0 & 0 & -1 & 0 & 1 & 0 & 0 \\ 0 & 0 & 0 & 1 & 0 & -1 & 0 & 0 & 1 \\ 0 & 0 & 0 & 1 & 0 & -1 & 0 & 0 & 0 \\ 0 & -1 & -1 & 0 & 1 & 0 & 0 & 1 & 0 \\ 1 & 0 & 0 & -1 & 0 & 1 & 0 & 0 & -1 \\ 0 & 1 & 1 & 0 & -1 & 0 & 0 & 0 & 0 \\ -1 & 0 & 0 & 0 & 0 & 0 & 0 & 0 & 0 \\ 0 & 0 & 0 & -1 & 0 & 0 & 0 & 0 & 0 \\ 0 & -1 & 0 & 0 & 1 & 0 & 0 & 0 & 0 \end{bmatrix} \begin{bmatrix} i_{b1} \\ u_{b2} \\ u_{b3} \\ i_{b4} \\ u_{b5} \\ i_{b6} \\ u_{b7} \\ u_{b8} \\ i_{b9} \end{bmatrix}. \quad (4)$$

In (4), the section in blue indicates the voltage relationship and can be obtained directly from (3). The section in red indicates the current relationship in the circuit and is obtained by anti-symmetric supplement. There is no need to analyze loop-branch incidence matrix anymore.

The proof of Lemma 1 can be conducted by the use of duality principle. However, this will make the proving process complicated. This paper provides a new approach of proof which is easy to understand.

*Proof:* First, replace all voltage and current sources with a uniform representation which has a constant resistor in parallel with a companion current source, as shown in Fig. 1(c). Then, every branch voltage can be written as a linear combination of

those companion current sources. Because the resistors in the network are constants, the coefficients of those linear combinations are also constants.

Second, set the value of all resistors to be 1 and write the following matrix equation:

$$\mathbf{u}_b = \mathbf{M}_1 \mathbf{I}_b \quad (5)$$

where  $\mathbf{u}_b$  is the branch voltage vector,  $\mathbf{I}_b$  is the companion current source vector, and  $\mathbf{M}_1$  is a  $b \times b$  constant symmetric matrix. By analyzing the relationship of branch voltage and current, the following equation can be written:

$$i_{bx} = u_{bx}/R_{bx} + I_{bx} \quad (6)$$

where  $x$  is the index number of branch. Because the value of all resistors in the network is 1, (6) can be written as

$$i_{bx} = u_{bx} + I_{bx}. \quad (7)$$

Then, the branch current vector can be expressed as

$$\mathbf{i}_b = \mathbf{M}_2 \mathbf{I}_b. \quad (8)$$

Matrix  $\mathbf{M}_1$  and  $\mathbf{M}_2$  have very similar form; their off-diagonal elements are the same and their diagonal elements differ by 1, or in matrix form

$$\mathbf{M}_2 = \mathbf{M}_1 + \mathbf{I} \quad (9)$$

where  $\mathbf{I}$  is the identity matrix.

Third, reorder the index of branch number so that the first  $n - 1$  branches are voltage sources and the latter  $b - n + 1$  branches are current sources. Then, the following matrix equation can be obtained:

$$\begin{bmatrix} u_{b(n-1)} \\ i_{b(b-n+1)} \end{bmatrix} = \mathbf{M} \mathbf{I}_b \quad (10)$$

where the first  $n - 1$  rows of  $\mathbf{M}$  are the same with the first  $n - 1$  rows of  $\mathbf{M}_1$  and the last  $b - n + 1$  rows of  $\mathbf{M}$  are the same with the last  $b - n + 1$  rows of  $\mathbf{M}_2$ . It is obvious that  $\mathbf{M}$  is also a symmetric matrix since it differs with  $\mathbf{M}_1$  and  $\mathbf{M}_2$  only on diagonal elements.

Fourth, invert matrix  $\mathbf{M}$  and (10) can be rewritten as

$$\mathbf{I}_b = \begin{bmatrix} \mathbf{M}_{11}^{-1} & \mathbf{M}_{12}^{-1} \\ \mathbf{M}_{21}^{-1} & \mathbf{M}_{22}^{-1} \end{bmatrix} \begin{bmatrix} u_{b(n-1)} \\ i_{b(b-n+1)} \end{bmatrix} = \mathbf{M}^{-1} \begin{bmatrix} u_{b(n-1)} \\ i_{b(b-n+1)} \end{bmatrix}. \quad (11)$$

Equation (11) reveals that the companion current source vector  $\mathbf{I}_b$  can also be expressed by the selected  $n - 1$  voltage sources and  $b - n + 1$  current sources. More importantly, the companion current source of every branch is simply the difference of branch current and voltage, as shown in the following:

$$I_{bx} = i_{bx} - u_{bx} \quad (12)$$

which means (11) has a similar form with (4). Let us denote the matrix in (4) as  $\mathbf{T}$  and the reordered form (where the first  $n - 1$  rows represent current relation and the last  $b - n + 1$  rows represent voltage relation) as  $\bar{\mathbf{T}}$ . To convert from  $\bar{\mathbf{T}}$  to  $\mathbf{M}^{-1}$ , let us consider in this way: for the  $n - 1$  voltage sources, their current value  $i_{bx}$  can be obtained by  $\bar{\mathbf{T}}$ , when

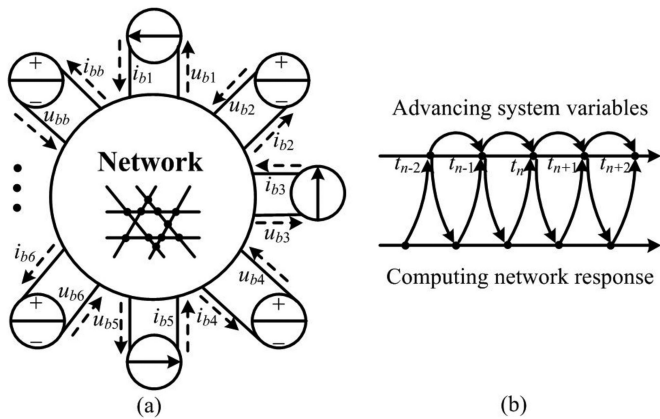


Fig. 2. EZM's working principle. (a) Configuration in space. (b) Configuration in time.

placing one additional  $-1$  on the diagonals of  $\mathbf{M}_{11}^{-1}$  and placing these  $\bar{\mathbf{T}}$  elements in  $\mathbf{M}_{12}^{-1}$ , their companion current sources  $I_{bx}$  are obtained; for the  $b - n + 1$  current sources, their voltage value  $u_{bx}$  can be obtained by  $\bar{\mathbf{T}}$ , when multiplying  $-1$  with these  $\bar{\mathbf{T}}$  elements and placing them in  $\mathbf{M}_{21}^{-1}$  and placing one additional  $1$  on the diagonals of  $\mathbf{M}_{22}^{-1}$ , their companion current sources  $I_{bx}$  are obtained. As mentioned previously, matrix  $\mathbf{M}$  is a symmetric matrix and so does  $\mathbf{M}^{-1}$ , then  $\mathbf{M}_{12}^{-1} = (\mathbf{M}_{21}^{-1})'$  and  $\bar{\mathbf{T}} = -\bar{\mathbf{T}}'$ . That is where the antisymmetry of matrix  $\mathbf{T}(\bar{\mathbf{T}})$  comes from.

It has to be mentioned that the reordering operation in step 3 is not necessary in the proving process and will not affect the antisymmetry of  $\mathbf{T}(\bar{\mathbf{T}})$ . The only reason for doing so is for better understanding. This proving process can be applied to any circuit topology, so Lemma 1 is a general rule.

Based on the above analysis, the EZM modeling methodology takes branch voltage/current as the computational variables. Given a circuit that has  $n$  nodes and  $b$  branches, EZM always selects  $n - 1$  branches and takes their voltages as system variables, and takes the remaining  $b - n + 1$  branches's currents as system variables. The updating of system variables can be divided into two interleaved processes, which are as follows:

- 1) advancing the system variables according to components' characteristics;
- 2) taking into account the influence of the system network.

The working principle of EZM can be illustrated in Fig. 2.

For the  $n - 1$  voltage source branches, they feed the network with their voltages and the network solver feeds them back with current values; for the  $b - n + 1$  current source branches, they feed the network with their currents and the network solver feeds them back with voltage values. This work is accomplished by using Lemma 1. As can be seen, once matrix  $\mathbf{T}$  is developed, the feedbacks of network is just simply addition/subtraction of the input system variables. The components can then utilize the response of network to update their values at next time-step.

There are a few things that have to be mentioned about EZM's working principle, which are as follows.

- 1) The most significant feature of EZM is the decoupling of circuit topology and components' characteristics. The

variations of components' characteristics will not affect the processing of circuit topology and the same is true vice versa. In most cases, the circuit topology remains unchanged during simulation and there is no need to invert matrix repeatedly.

- 2) Even in cases when the circuit topology changes with time (like circuit breakers and switches), the development of matrix  $\mathbf{T}$  is relatively easy and suitable for computer programming. The only computational complexity comes from the inversion of matrix  $\mathbf{A}'_1$ . Two features of  $\mathbf{A}'_1$  make this task easy. First, the elements of  $\mathbf{A}'_1$  have only three possible values:  $0$  or  $\pm 1$  and there are at most two nonzero values in each row; second, when the corresponding node of deleted row in  $\mathbf{A}$  has at least one voltage source connected to it, then there is at least one row in  $\mathbf{A}'_1$  that has only one nonzero value.
- 3) The processing of individual components is also decoupled from each other. As can be seen in Fig. 2, the network receives system variables at time  $t_{n-1}$  and feeds back to components at time  $t_n$ . The feedbacks are used by components at time  $t_n$ , which means the component is using the previous time-step system variables to compute the current time-step value. This kind of configuration will be definitely detrimental to the numerical stability and accuracy of the model. But this phenomena can be alleviated by better numerical algorithms and smaller time-steps, which will be analyzed in the next section. However, it does not mean this design is unreasonable. Actually, it is believed that it is a more natural way to simulate the behavior of circuits. From the point view of component itself, it does not care what kind of topology or vicinity components it connects to. It just behaves as its own way and can be viewed as the consequence of constantly interacting between component's input/output voltage and current. The only difference is that this interaction process in reality happens simultaneously or at an infinite small time-step.
- 4) The decoupling of circuit topology and every individual component makes EZM extremely suitable for parallel computation. If the computational cost of developing matrix  $\mathbf{T}$  is neglected, the overall computational complexity of EZM becomes linear or  $O(N)$ , and if fully parallel computation is achieved, the computational complexity even reduces to  $O(1)$  in respect of computation time, i.e., constant computational complexity, which makes real-time simulation and smaller time-step possible.
- 5) High scalability is achieved in EZM as when adding or removing one branch from the network, it is not necessary to remodel the system from scratch. The matrix that represents the remaining part of network is still useful and can be scaled up/down.
- 6) Hierarchical design is inherently embedded in EZM. As can be seen that every branch is represented by voltage or current source; there is no restriction about the inner structure of branch at all. In other words, the equivalent voltage or current source in upper level may contain multiple lower level voltage and current sources as long as

TABLE I  
SOME CONVENTIONS OF CIRCUIT COMPONENTS

Voltage-source-like	Current-source-like
Resistors, Capacitors, Batteries, Generators Switches in turn-on transients and steady on-state	Resistors, Inductors, PV panels, Motors, Switches in turn-off transients and steady off-state

the interface with upper level remains the same. The inner variation in lower level will not affect the computation of upper level and they can even be solved using traditional nodal analysis or state-space method. This feature provides great facility for system partitioning.

7) Multirate computation is convenient in EZM. Due to the decoupling nature of each individual component, every component can have its own simulation time-step and will not affect each other. Each row of matrix  $\mathbf{T}$  represents the computation in network solver corresponding to one component. They can work along with individual component's rate and do not necessarily have the same time-step. This feature is very useful in practice because different components in the circuit have different inertia and require different time-steps.

8) The choice of each component being viewed as voltage or current source is a big issue. Although no standard way for determining this is available, there are still some empirical practices which can serve as guidelines. Table I lists some common circuit components and their conventions.

Based on the above classification, some treatments have to be taken to avoid circuit contentions. For example, when two capacitors connect in parallel, they should be merged into one to avoid two voltage sources connected in parallel. The same is true for series connected inductors. Special attention should be given to resistors as they can be viewed as either voltage source or current source. It depends on the circuit configuration. When the resistor connects in parallel with a voltage source, then it should be viewed as a current source; when it connects in series with a current source, then it should be viewed as a voltage source. In addition, EZM is not suitable for solving a pure resistor network. The reason is that one cannot write a formula about the gradient of resistor's voltage or current. In other words, the transient frequency of resistor can be infinitely high which is beyond the computation ability of EZM. As a result, the transients of resistor should be incorporated with other circuit components and all the directly parallel and series connected resistors should be merged. Fortunately, this task is not hard to achieve.

9) Three-phase system is very important in modern power systems and it is treated slightly different in EZM. It is well known that a  $n$  ports network has only  $n - 1$  independent output voltages or currents. The three-phase voltage/current source should be treated as two independent voltage/current sources in EZM unless the neutral point also connects out, as shown in Fig. 3.

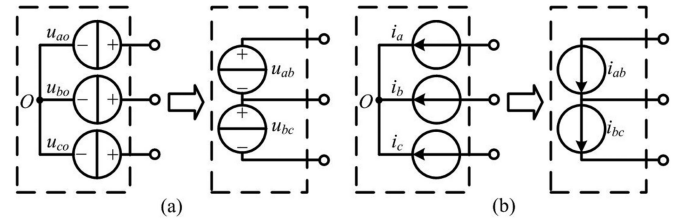


Fig. 3. Three-phase voltage/current equivalent configuration in EZM. (a) Voltage source configuration. (b) Current source configuration.

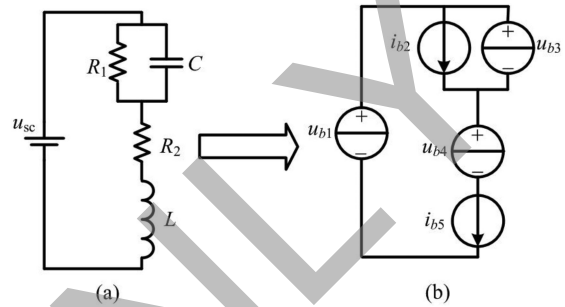


Fig. 4. Numerical stability analysis example. (a) Circuit configuration. (b) Equivalent circuit in EZM.

As a result, the commonly used abc/dq coordinate transformation in EZM is slightly different with traditional one

$$\begin{bmatrix} x_d \\ x_q \\ x_o \end{bmatrix} = \frac{2}{3\sqrt{3}} \begin{bmatrix} \cos(\theta + \frac{\pi}{6}) & \cos(\theta - \frac{\pi}{2}) & \cos(\theta + \frac{5}{6}\pi) \\ -\sin(\theta + \frac{\pi}{6}) & -\sin(\theta - \frac{\pi}{2}) & -\sin(\theta + \frac{5}{6}\pi) \\ \frac{1}{2} & \frac{1}{2} & \frac{1}{2} \end{bmatrix} \times \begin{bmatrix} x_{ab} \\ x_{bc} \\ x_{ca} \end{bmatrix} \quad (13)$$

where  $x_{ca} = -x_{ab} - x_{bc}$  is not an independent source.

### III. NUMERICAL STABILITY ANALYSIS AND RELATION BETWEEN EZM AND NODAL ANALYSIS AND STATE-SPACE METHOD

This section uses a simple RLC circuit [shown in Fig. 4(a)] to analyze the numerical stability of EZM and its relation with nodal analysis and state-space method.

First, using the state-space method routine to solve the system, the following state-space equations can be obtained:

$$\begin{bmatrix} \frac{du_C}{dt} \\ \frac{di_L}{dt} \end{bmatrix} = \begin{bmatrix} -\frac{1}{R_1 C} & \frac{1}{C} \\ -\frac{1}{L} & -\frac{R_2}{L} \end{bmatrix} \begin{bmatrix} u_C \\ i_L \end{bmatrix} + \begin{bmatrix} 0 \\ \frac{1}{L} \end{bmatrix} u_{sc} \quad (14)$$

where the voltage of capacitor  $u_C$  and the current of inductor  $i_L$  are selected as state variables.

When discretized using the forward Euler method, (14) can be rewritten as follows:

$$\begin{bmatrix} u_C(t_n) \\ i_L(t_n) \end{bmatrix} = \begin{bmatrix} 1 - \frac{\Delta t}{R_1 C} & \frac{\Delta t}{C} \\ -\frac{\Delta t}{L} & 1 - \frac{R_2 \Delta t}{L} \end{bmatrix} \begin{bmatrix} u_C(t_{n-1}) \\ i_L(t_{n-1}) \end{bmatrix} + \begin{bmatrix} 0 \\ \frac{\Delta t}{L} \end{bmatrix} u_{sc} \quad (15)$$

where  $\Delta t = t_n - t_{n-1}$  is the time-step.

Second, solving the same system using EZM. The equivalent circuit is shown in Fig. 4(b). There are five branches in total and the corresponding matrix  $\mathbf{T}$  can be obtained using Lemma 1,

$$\begin{bmatrix} \dot{i}_{b1} \\ u_{b2} \\ i_{b3} \\ \dot{i}_{b4} \\ u_{b5} \end{bmatrix} = \begin{bmatrix} 0 & 0 & 0 & 0 & -1 \\ 0 & 0 & 1 & 0 & 0 \\ 0 & -1 & 0 & 0 & 1 \\ 0 & 0 & 0 & 0 & 1 \\ 1 & 0 & -1 & -1 & 0 \end{bmatrix} \begin{bmatrix} u_{b1} \\ i_{b2} \\ u_{b3} \\ u_{b4} \\ i_{b5} \end{bmatrix}. \quad (16)$$

According to each component's characteristics, the system variables should be renewed in the following way:

$$\begin{aligned} u_{b1}(t_n) &= u_{sc} \\ i_{b2}(t_n) &= \frac{u_{b2}(t_{n-1})}{R_1} \\ u_{b3}(t_n) &= u_{b3}(t_{n-1}) + \frac{\Delta t}{C} i_{b3}(t_{n-1}) \\ u_{b4}(t_n) &= R_2 i_{b4}(t_{n-1}) \\ i_{b5}(t_n) &= i_{b5}(t_{n-1}) + \frac{\Delta t}{L} u_{b5}(t_{n-1}) \end{aligned} \quad (17)$$

where the capacitor voltage and inductor current are also discretized using the forward Euler method. When incorporating with (16),  $u_{b3}(t_n)$  and  $i_{b5}(t_n)$  can also be written as follows:

$$\begin{aligned} u_{b3}(t_n) &= \left(1 - \frac{\Delta t}{R_1 C}\right) u_{b3}(t_{n-1}) + \frac{\Delta t}{C} i_{b5}(t_{n-1}), \\ i_{b5}(t_n) &= \left(1 - \frac{R_2 \Delta t}{L}\right) i_{b5}(t_{n-1}) - \frac{\Delta t}{L} u_{b3}(t_{n-1}) + \frac{\Delta t}{L} u_{sc} \end{aligned} \quad (18)$$

which is exactly the same with (15). In other words, the numerical stability of solving the system using (16) and (17) is exactly the same with (15). To find the eigenvalues of (15), the following equation should be solved:

$$\left[ z - \left(1 - \frac{\Delta t}{R_1 C}\right) \right] \left[ z - \left(1 - \frac{R_2 \Delta t}{L}\right) \right] + \frac{\Delta t^2}{LC} = 0. \quad (19)$$

To make the eigenvalues locate inside the unit circle, the absolute term of (19) should be less than 1, i.e.,

$$\left(1 - \frac{\Delta t}{R_1 C}\right) \left(1 - \frac{R_2 \Delta t}{L}\right) + \frac{\Delta t^2}{LC} < 1. \quad (20)$$

It can be observed that the first term in (20) is always less 1, provided that the second term is small enough, then the whole expression will be less than 1. In other words, as long as the time-step  $\Delta t$  is small enough, the above solver is stable.

Actually, lowering the time-step is not the only way to enhance the numerical stability of EZM. Another way is using better numerical algorithm. As mentioned before, the solver uses previous time-step system variables to compute the current time-step value. In numerical algorithm area, this means the employment of an explicit method. Explicit method means all the system variables are totally determined from previous time-step values and there is no influence between current time-step values. In this manner, the matrix inversion is saved. The implicit

method, however, takes into account the interaction effect of system variables at each time-step and matrix inversion is required. This is why the implicit method is always unconditionally numerical stable, while explicit method is always conditionally stable. For example, the Tustin method (or trapezoidal method) always maps the left half-plane zone in continuous domain to the inner unit circle zone in discrete domain and this is what nodal analysis method's computation approach. There are various explicit methods that can be found in literature and they are all suitable to be employed in EZM. Among them, the Heun method (also known as modified trapezoidal method or improved Euler method) and the Runge–Kutta method are good choices. The fourth-order Runge–Kutta method makes a good balance between numerical performance and computational load. It will serve as the numerical discretization method in the following test case.

#### IV. REAL-TIME APPLICATION OF EZM ON MORE ELECTRIC AIRCRAFT MICROGRID

More electric aircraft (MEA) is deemed as next generation aircraft to help simplify system structure, improve reliability, and save fuel [21]–[27]. The Boeing-787 is equipped with a large-scale electric power system to eliminate the traditional pneumatic system and bleed manifold, which is called “No-Bleed Systems” by the company [28]. This section applies the EZM to build a real-time system of the Boeing-787 microgrid (shown in Fig. 5) to testify the validity and computational efficiency of EZM.

Real-time application of a large and complicated system like MEA microgrid is difficult to achieve using conventional modeling methods because of their high computational complexity. However, by utilization of EZM modeling methodology, this task becomes relatively easy because the whole system can be dealt in a divide and conquer manner. The MEA microgrid is constructed at component level first where the corresponding characteristics can be found in literature. Then, these components are treated as either voltage or current sources and assembled into a network in hierarchical and zonal fashion. Thereby, the EZM's computation principle can be applied to solve the network state. When combined with field programmable gate array (FPGA) where highly parallel computation is available, the real-time simulation of Boeing-787 MEA microgrid is realized. The numerical stability analysis presented in the previous section assures that by employment of proper numerical discretization method and small time step (the fourth-order Runge–Kutta method at 1  $\mu$ s time-step in this study case), the whole simulation model is computational safe and accurate.

The hardware configuration of the real-time MEA emulation system is shown in Fig. 6. The transient waveforms are calculated digitally in real-time on Xilinx Virtex UltraScale+VCU118-ES1 FPGA evaluation platform and exported to oscilloscope through a digital-to-analog converter for display. There are multiple communication interfaces between the FPGA board and the external computer so that the hardware-in-the-loop (HIL) emulation is available on this test set-up. The microgrid model of MEA with exact the same structure in Fig. 5 is built on the FPGA hardware while some controllers can be

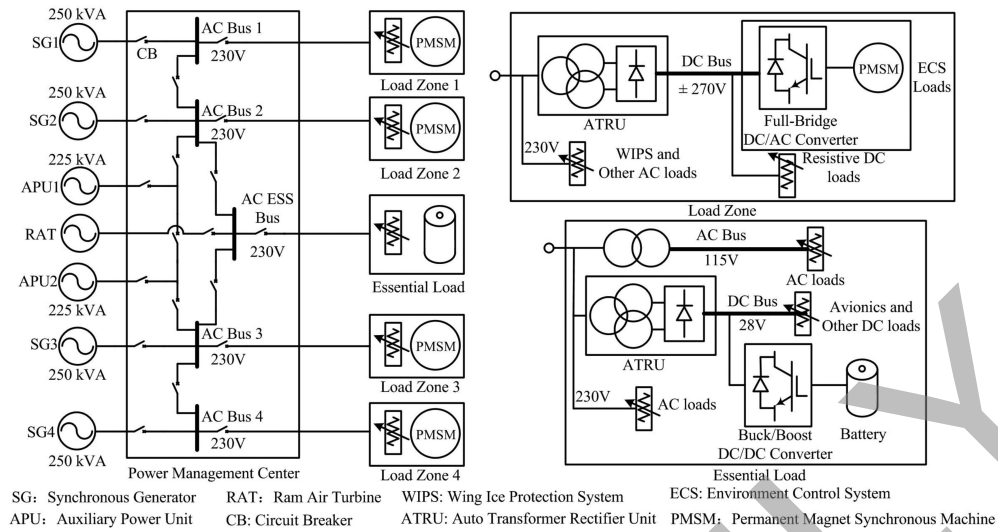


Fig. 5. Structure of Boeing-787 microgrid.

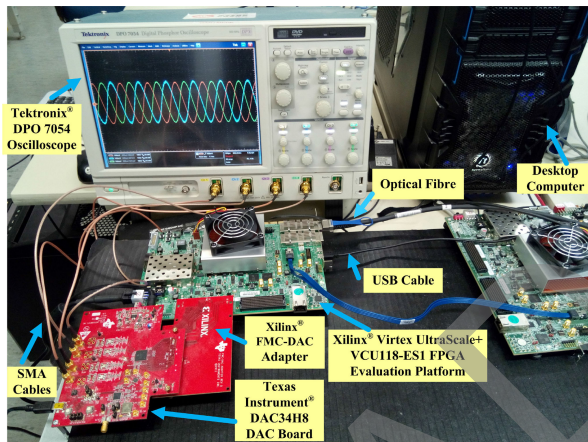


Fig. 6. Hardware configuration of the real-time MEA emulation system.

put on the external computer for performance validation and parameter design because it is very convenient to tune controller parameters on the computer. On the other hand, it is also convenient to modify the structure or component value of the MEA microgrid model. The only effort is to resynthesize the model and download it to the FPGA board.

In order to assess the accuracy and validity of the above test set-up, the same study case is also developed in PSCAD/EMTDC and the results are used for comparison.

### A. Normal Operation Test Scenarios

Two test scenarios under normal working operation are presented in this subsection.

**1) Abrupt Load Change of WIPS:** Wind ice protection system (WIPS) load is one of the major loads in the 230 V ac bus. The WIPS is not always working under full load and when there is an abrupt load change, it will have significant influence on ac and dc bus. Fig. 7 presents the transient waveforms when the ac bus1 load changes from 33.12 to 63.96 kW at  $t = 0.1$  s and changes back at  $t = 0.12$  s because of WIPS load fluctuation.

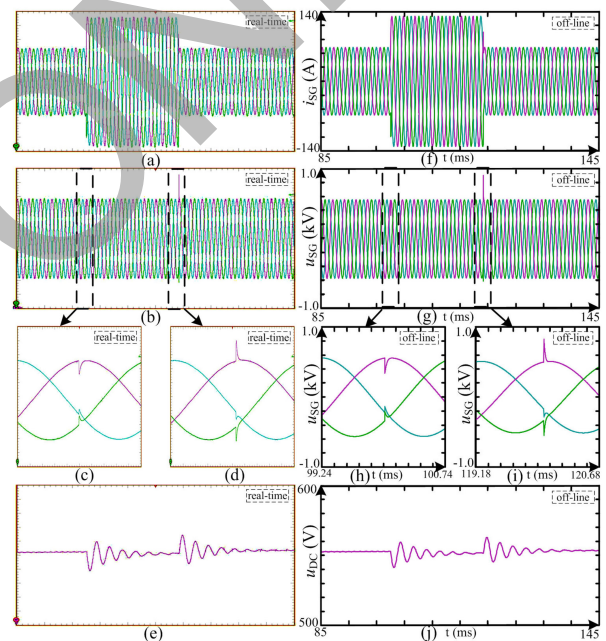
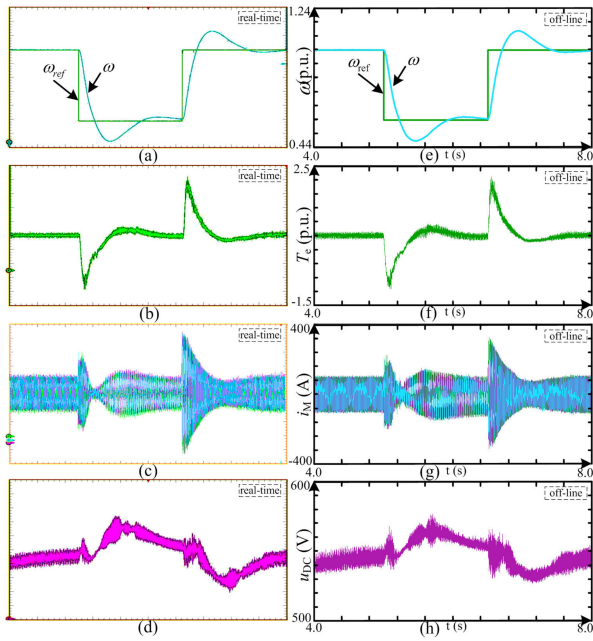


Fig. 7. Transient waveforms under WIPS abrupt load change. (a) Generator line currents  $i_{SG}$  from EZM, y-axis: 28 A/div, x-axis: 6 ms/div. (b) Generator line-line voltages  $u_{SG}$  from EZM, y-axis: 200 V/div, x-axis: 6 ms/div. (c) and (d) Magnified waveforms of (b), y-axis: 200 V/div, x-axis: 150  $\mu$ s/div. (e) DC bus voltage  $u_{DC}$  from EZM, y-axis: 10 V/div,  $t$ -offset: 550 V, x-axis: 6 ms/div. (f)–(j) Counterparts of (a)–(e) from PSCAD/EMTDC with the same axis scale.

Both the ac and dc bus have sensed the load change and voltage transients are induced.

**2) PMSM Speed Regulation Transients:** Permanent magnet synchronous machine (PMSM) is utilized mainly for environment control, which helps to keep the temperature and air pressure in the aircraft cabin within reasonable range. For a better control precision and fuel saving purpose, closed-loop speed regulation of PMSM is necessary. Fig. 8 presents the waveforms when the speed command  $\omega_{ref}$  of PMSM jumps from 1.0 to 0.6 p.u. at  $t = 5.0$  s and increases back to 1.0 p.u. at  $t = 6.5$  s (the load torque applied to PMSM is 0.5 p.u.). It can be



**Fig. 8.** Transient waveforms of PMSM speed regulation. (a) Speed command  $\omega_{ref}$  and motor speed  $\omega$  from EZM, y-axis: 0.08 p.u./div, y-offset: 0.84 p.u., x-axis: 400 ms/div. (b) Motor torque  $T_e$  from EZM, y-axis: 0.4 p.u./div, y-offset: 0.5 p.u., x-axis: 400 ms/div. (c) Motor currents  $i_M$  from EZM, y-axis: 80 A/div, x-axis: 400 ms/div. (d) DC bus voltage  $u_{DC}$  from EZM. y-axis: 10 V/div, y-offset: 550 V, x-axis: 400 ms/div. (e)–(h) Counterparts of (a)–(d) from PSCAD/EMTDC with the same axis scale.

noticed that the speed, torque as well as motor currents have experienced obvious transients and stabilized in about 1.5 s. The dc bus voltage is also affected by the motor transients but within the reasonable range. Because of the power electronic dc–ac converter, the dc bus voltage have abundant high-frequency components. The results from EZM and PSCAD/EMTDC have very high consistency.

## B. Fault Operation Test Scenarios

The safety of aircraft can not be overemphasized in the aviation industry. This requires the MEA microgrid to have very high reliability. It should have the ability to get through or recover from fault condition. Two test scenarios under fault conditions are presented in this subsection.

**1) Line-Line Fault of ac Bus:** AC bus is crucial to the aircraft power system as it is the link that connects the power sources and loads. Fig. 9 presents the transient waveforms of ac bus voltages and currents as well as dc bus voltage when there is a phase A–B line–line fault at  $t = 0.2$  s and cleared at  $t = 0.22$  s. The ac system comes to asymmetry operating condition and the dc bus voltage drops during fault. When the fault is cleared, the ac system comes back to normal mode and dc bus voltage also recovers. This demonstrates that the MEA power system has the ability to get through fault.

**2) Loss of SG:** The four load zones work independently under normal condition because of variable frequency of individual ac bus (320–800 Hz). However, when one generator encounters a failure and is disconnected from the ac bus, the power management center should transfer the corresponding load to another ac bus. Fig. 10 presents the transient waveforms

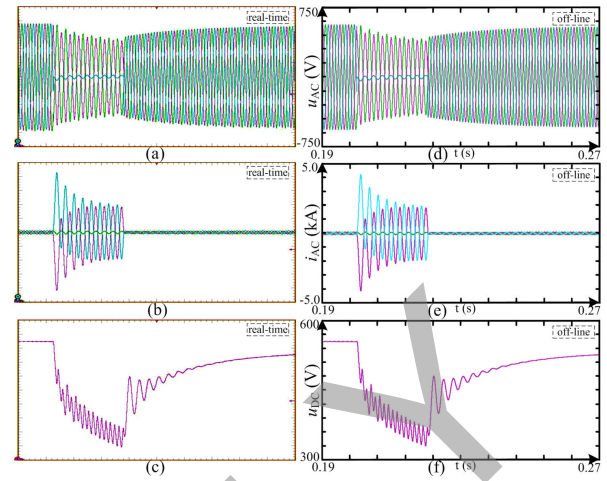


**Fig. 9.** Transient waveforms of ac bus line-line fault. (a) AC bus line-line voltages  $u_{AC}$  from EZM, y-axis: 150 V/div, x-axis: 8 ms/div. (b) AC bus line currents  $i_{AC}$  from EZM, y-axis: 1000 A/div, x-axis: 8 ms/div. (c) DC bus voltage  $u_{DC}$  from EZM. y-axis: 30 V/div, y-offset: 450 V, x-axis: 8 ms/div. (d)–(f) Counterparts of (a)–(c) from PSCAD/EMTDC with the same axis scale.

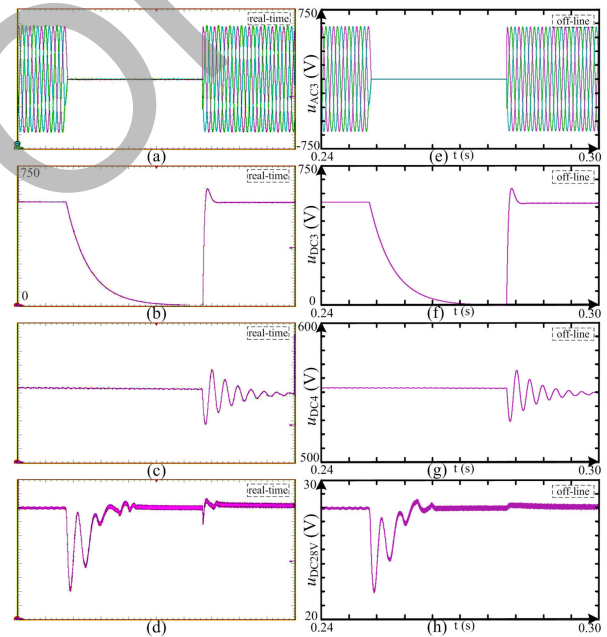


**Fig. 10.** Transient waveforms of SG loss fault. (a) AC bus 3 line-line voltages  $u_{AC3}$  from EZM, y-axis: 150 V/div, x-axis: 6 ms/div. (b) DC bus 3 voltage  $u_{DC3}$  from EZM, y-axis: 75 V/div, y-offset: 375 V, x-axis: 6 ms/div. (c) DC bus 4 voltage  $u_{DC4}$  from EZM, y-axis: 10 V/div, y-offset: 550 V, x-axis: 6 ms/div. (d) DC 28 V bus voltage  $u_{DC28V}$  from EZM, y-axis: 1 V/div, y-offset: 25 V, x-axis: 6 ms/div. (e) and (f) Counterparts of (a)–(d) from PSCAD/EMTDC with the same axis scale.

when SG3 is disconnected from ac bus 3 at  $t = 0.25$  s and the power management center transfers load zone 3 to ac bus 4 at  $t = 0.28$  s. As can be seen that dc bus 3 voltage drops to zero during failure but backs to normal value after ac voltages recover. In the meantime, dc bus 4 voltage is also affected by the load transfer but stabilized shortly. As comparison, the dc 28 V bus is essential to the avionics and is equipped with energy storage compensation dc–dc converter. When faced with the same ac power source loss condition, the dc 28 V bus voltage

does not drop to zero and recovers very quickly because of the compensating energy from battery.

The above simulation waveforms can be used to check the validity of MEA microgrid. This real-time simulation model is suitable for HIL testing to make sure all the transients meet some specific industrial or military standards like MIL-STD-704F. More detailed waveforms including device-level switching transients are also available but omitted due to page limitation.

## V. CONCLUSION

This paper presented an efficient method which is very suitable for large-scale circuit simulation. The proposed method was based on a circuit lemma, which indicated the relationship of branch voltages and currents. By utilization of this lemma, the circuit topology and components' characteristics are decoupled and the computational complexity reduces to nearly linear. The proposed method was verified by a study case that comes from the MEA microgrid and HIL testing of normal and fault operation scenarios were realized on FPGA board. Output waveforms from EZM were compared with PSCAD/EMTDC results and showed very high consistency. The good performance on computational accuracy and efficiency demonstrated that EZM could be a good alternative for modeling large and complex systems. The implementation of EZM on MEA microgrid provided great facility for system design and performance validation.

## REFERENCES

- [1] X. Guillaud *et al.* "Applications of real-time simulation technologies in power and energy systems," *IEEE Power Energy Technol. Syst. J.*, vol. 2, no. 3, pp. 103–115, Sep. 2015.
- [2] M. D. O. Faruque *et al.* "Real-time simulation technologies for power systems design, testing, and analysis," *IEEE Power Energy Technol. Syst. J.*, vol. 2, no. 2, pp. 63–73, Jun. 2015.
- [3] H. W. Dommel, "Digital computer solution of electromagnetic transients in single- and multiphase networks," *IEEE Trans. App. Syst.*, vol. PAS-88, no. 4, pp. 388–399, Apr. 1969.
- [4] C.-W. Ho, A. Ruehli, and P. Brennan, "The modified nodal approach to network analysis," *IEEE Trans. Circuits Syst.*, vol. 22, no. 6, pp. 504–509, Jun. 1975.
- [5] K. Strunz and E. Carlson, "Nested fast and simultaneous solution for time-domain simulation of integrative power-electric and electronic systems," *IEEE Trans. Power Del.*, vol. 22, no. 1, pp. 277–287, Jan. 2007.
- [6] M. A. Elizondo, F. K. Tuffner, and K. P. Schneider, "Simulation of inrush dynamics for unbalanced distribution systems using dynamic-phasor models," *IEEE Trans. Power Syst.*, vol. 32, no. 1, pp. 633–642, Jan. 2016.
- [7] L. O. Chua and P. M. Lin, *Computer Aided Analysis of Electronic Circuits: Algorithms and Computational Techniques*, Englewood Cliffs, CA, USA: Prentice-Hall, 1975.
- [8] L. A. Grgoire, H. F. Blanchette, J. Blanger, and K. Al-Haddad, "A stability and accuracy validation method for multirate digital simulation," *IEEE Trans. Ind. Inf.*, vol. 13, no. 2, pp. 512–519, Apr. 2017.
- [9] L. A. Dessaint, K. Al-Haddad, H. Le-Huy, G. Sybille, and P. Brunelle, "A power system simulation tool based on Simulink," *IEEE Trans. Ind. Electron.*, vol. 46, no. 6, pp. 1252–1254, Dec. 1999.
- [10] A. Davoudi, J. Jatskevich, and T. De Rybel, "Numerical state-space average-value modeling of PWM dc–dc converters operating in DCM and CCM," *IEEE Trans. Power Electron.*, vol. 21, no. 4, pp. 1003–1012, Jul. 2006.
- [11] J. A. R. Macias, A. G. Exposito, and A. B. Soler, "A comparison of techniques for state-space transient analysis of transmission lines," *IEEE Trans. Power Del.*, vol. 20, no. 2, pp. 894–903, Apr. 2005.
- [12] H. F. Blanchette, T. Ould-Bachir, and J. P. David, "A state-space modeling approach for the FPGA-based real-time simulation of high switching frequency power converters," *IEEE Trans. Ind. Electron.*, vol. 59, no. 12, pp. 4555–4567, Dec. 2012.
- [13] *EMTDC User's Guide Version 4.2.0*, Manitoba HVDC Research Center, Winnipeg, MB, Canada, 2005.
- [14] *Simulink User's Guide (R2016a)*, The MathWorks, Inc., Natick, MA, USA, 2016.
- [15] J. E. Schutt-Aine, "Latency insertion method (LIM) for the fast transient simulation of large networks," *IEEE Trans. Circuits Syst. I: Fundam. Theory Appl.*, vol. 48, no. 1, pp. 81–89, Jan. 2001.
- [16] A. Benigni, A. Monti, and R. A. Dougal, "Latency-based approach to the simulation of large power electronics systems," *IEEE Trans. Power Electron.*, vol. 29, no. 6, pp. 3201–3213, Jun. 2014.
- [17] S. N. Lalgudi, M. Swaminathan, and Y. Kretchmer, "On-chip power-grid simulation using latency insertion method," *IEEE Trans. Circuits Syst. I, Reg. Papers.*, vol. 55, no. 3, pp. 914–931, Apr. 2008.
- [18] S. Y. R. Hui, K. K. Fung, and C. Christopoulos, "Decoupled simulation of multi-stage power electronic systems using transmission-line links," in *Proc. Rec. IEEE Power Electron. Specialists Conf.*, Toledo, Spain, 1992, pp. 1324–1330.
- [19] S. Y. R. Hui and K. K. Fung, "Fast decoupled simulation of large power electronic systems using new two-port companion link models," *IEEE Trans. Power Electron.*, vol. 12, no. 3, pp. 462–473, May 1997.
- [20] Z. Huang and V. Dinavahi, "A fast and stable method for modeling generalized nonlinearities in power electronic circuit simulation and its real-time implementation," *IEEE Trans. Power Electron.*, to be published, doi: 10.1109/TPEL.2018.2851570.
- [21] P. Wheeler and S. Bozhko, "The more electric aircraft: Technology and challenges," *IEEE Electrific. Mag.*, vol. 2, no. 4, pp. 6–12, Dec. 2014.
- [22] B. Sarlioglu and C. T. Morris, "More electric aircraft: Review, challenges, and opportunities for commercial transport aircraft," *IEEE Trans. Transp. Electrific.*, vol. 1, no. 1, pp. 54–64, Jun. 2015.
- [23] S. V. Bozhko, T. Wu, Y. Tao, and G. M. Asher, "More-electric aircraft electrical power system accelerated functional modeling," in *Proc. 14th Int. Power Electron. Motion Control Conf.*, Ohrid, Macedonia, 2010, pp. T9-7–T9-14.
- [24] T. Yang, S. Bozhko, and G. Asher, "Functional modeling of symmetrical multipulse autotransformer rectifier units for aerospace applications," *IEEE Trans. Power Electron.*, vol. 30, no. 9, pp. 4704–4713, Sep. 2015.
- [25] A. Griffo, D. Drury and D. Salt, "Hardware in the loop based synchronous generator emulation test rig for more electric aircraft power systems," in *Proc. Int. Conf. Electr. Syst. Aircr., Railway Ship Propulsion*, Bologna, Oct. 2012, pp. 1–6.
- [26] K. Xu, N. Xie, C. Wang, and X. Shi, "Modeling and simulation of variable speed variable frequency electrical power system in more electric aircraft," *Open Elect. Electron. Eng. J.*, vol. 11, pp. 87–98, 2017.
- [27] E. Ganey, "Selecting the best electric machines for electrical power generation systems: High-performance solutions for aerospace more electric architectures," *IEEE Electrific. Mag.*, vol. 2, no. 4, pp. 13–22, Dec. 2014.
- [28] M. Sinnett, "787 no-bleed systems: Saving fuel and enhancing operational efficiencies," *Aeromagazine*, vol. 4, pp. 6–11, 2007.



**Zhen Huang** (S'18) received the B.Eng. degree in electrical engineering from Xi'an Jiaotong University, Xi'an, China, in 2012, and the M.Eng. degree in electrical engineering from Tsinghua University, Beijing, China, in 2015. He is currently working toward the Ph.D. degree in electrical engineering with the Department of Electrical and Computer Engineering, University of Alberta, Edmonton, AB, Canada.

He has two years work experience in the power electronics industry. His research interests include high-performance modeling and simulation of power electronics and power systems.



**Venkata Dinavahi** (SM'08) received the B.Eng. degree in electrical engineering from the Visvesvaraya National Institute of Technology, Nagpur, India, in 1993, the M.Tech degree in electrical engineering from the Indian Institute of Technology Kanpur, Kanpur, India, in 1996, and the Ph.D. degree in electrical and computer engineering from the University of Toronto, Toronto, ON, Canada, in 2000.

He is currently a Professor with the Department of Electrical and Computer Engineering, University of Alberta, Edmonton, AB, Canada. His research interests include real-time simulation of power systems and power electronic systems, electromagnetic transients, device-level modeling, large-scale systems, and parallel and distributed computing.